AMERICAN UNIVERSITY OF BEIRUT

AFFINELY ADJUSTABLE ROBUST COUNTERPART APPROACH FOR LOCAL DISPATCHING OF THE INVERTER'S REACTIVE POWER

by
ISSAM NAYEF MOUSA

A thesis
submitted in partial fulfillment of the requirements
for the degree of Master of Engineering
to the Department of Electrical and Computer Engineering
of Maroun Semaan Faculty of Engineering and Architecture
at the American University of Beirut

Beirut, Lebanon
May 2018

AMERICAN UNIVERSITY OF BEIRUT

AFFINELY ADJUSTABLE ROBUST COUNTERPART APPROACH FOR LOCAL DISPATCHING OF THE INVERTER'S REACTIVE POWER

by

ISSAM NAYEF MOUSA

Approved by:

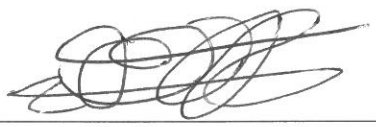

Dr. Rabih Jabr, Professor — Advisor
Electrical and Computer Engineering

Dr. Riad Chedid, Professor — Member of Committee
Electrical and Computer Engineering

Dr. Sami Karaki, Professor — Member of Committee
Electrical and Computer Engineering

Date of thesis defense: May 3, 2018

AMERICAN UNIVERSITY OF BEIRUT

THESIS, DISSERTATION, PROJECT RELEASE FORM

Student Name:

Mousa	Issam	Nayef
Last	First	Middle

⊗ Master's Thesis ○ Master's Project ○ Doctoral Dissertation

☐ I authorize the American University of Beirut to: (a) reproduce hard or electronic copies of my thesis, dissertation, or project; (b) include such copies in the archives and digital repositories of the University; and (c) make freely available such copies to third parties for research or educational purposes.

☒ I authorize the American University of Beirut, to: (a) reproduce hard or electronic copies of it; (b) include such copies in the archives and digital repositories of the University; and (c) make freely available such copies to third parties for research or educational purposes after:

One ---- year from the date of submission of my thesis, dissertation, or project.
Two ---- years from the date of submission of my thesis, dissertation, or project.
Three X- years from the date of submission of my thesis, dissertation, or project.

Signature

May 3, 2018

Date

ACKNOWLEDGMENTS

I can’t start writing this part without thanking my great supervisor Professor Rabih Jabr, for his positive support, mentorship, and approachability. His help and advice were invaluable in doing my research. Also, I would like to thank my other committee members, Professors Sami Karaki and Riad Chedid.

My recognition and gratitude are addressed to Abdullah Al Ghurair foundation for Education for their financial support to study at the American University of Beirut, and for their mentoring and advising.

Thanks to the Lebanese National Council of Scientific Research (LNCSR) and the American University of Beirut who funded my research project.

AN ABSTRACT OF THE THESIS OF

Issam Nayef Mousa for Master of Engineering
Major: Energy and Power Systems

Title: Affinely Adjustable Robust Counterpart Approach for Local Dispatching of the Inverter's Reactive Power

An electrical distribution system with high penetration levels of photovoltaic (PV) generation is exposed to degradation in power quality due to voltage fluctuation beyond the acceptable levels; this is caused by the rapidly varying generation levels from the PV generators possibly causing reverse power flows. Currently installed regulation equipment like under load-tap changing transformers, step voltage regulators, and switched capacitors are slow; they cannot provide an adequate response to the fast varying generation levels.

A proposed solution is the introduction of fast-reacting PV inverters that can consume or supply reactive power to account for the voltage sags and swells on the distribution network, and that also provide the network operators with the opportunity to optimize thermal losses.

This thesis presents an affinely adjustable robust counterpart (AARC) approach for the optimal local dispatch of reactive power from the PV inverters; it accounts for uncertainty in the photovoltaic generation levels and aims to minimize the maximum absolute voltage magnitude deviation from the nominal voltage level. Numerical results confirmed the effectiveness of the proposed approach in reducing both the maximum absolute voltage magnitude deviation and the system power loss.

CONTENTS

ILLUSTRATIONS

TABLES

NOMENCLATURE

A. Notation

$\bar{A}$	Complex value.
$\lvert\bar{A}\rvert$	Magnitude of $\bar{A}$.
$\boldsymbol{B}$	Matrix or vector $\boldsymbol{B}$.
$inv(\boldsymbol{B})$	Inverse of matrix $\boldsymbol{B}$.
B^i	Row i of matrix $\boldsymbol{B}$.
$\boldsymbol{diag}(\boldsymbol{v})$	Square diagonal matrix with the elements of vector $\boldsymbol{v}$ on the main diagonal.
$\boldsymbol{eye}(\boldsymbol{n})$	$n \times n$ identity matrix with ones on the main diagonal and zeros elsewhere.
$\boldsymbol{ones}(\boldsymbol{n}, \boldsymbol{1})$	$n \times 1$ matrix of ones.
$re(\boldsymbol{B})$, $imag(\boldsymbol{B})$	Real and imaginary parts of matrix $\boldsymbol{B}$.
$\boldsymbol{zeros}(\boldsymbol{n}, \boldsymbol{1})$	$n \times 1$ matrix of zeros.

B. Parameters, Vectors, & Variables

α_i	Constant term of the local control rule of the PV inverter at bus i.
γ_i	Slope of the local control rule of the PV inverter at bus i.
$d(i)$	Set of all descendants of node i excluding node i.

L_i	Set of all lines between bus 0 and bus i.
$\|\Delta V\|_\infty$	Maximum absolute voltage magnitude deviation in the network.
n	Number of nodes.
n_b	Number of branches
N	Set of all buses excluding bus 0.
P_i, Q_i	Real and reactive power flow out of bus i.
P_{Li}, Q_{Li}	Real and reactive power of the load at bus i.
p_i^g, p_i^c	PV real power generation and load real power consumption at bus i respectively.
$\boldsymbol{p^g}, \boldsymbol{p^c}$	Real power generation and consumption vectors of size $(n \times 1)$.
q_i^g, q_i^c	Inverter's reactive power and consumed reactive power by the load at bus i.
$\boldsymbol{q^g}, \boldsymbol{q^c}$	Reactive power generation and consumption vectors of size $(n \times 1)$.
r_i, x_i	Resistance and reactance of the line departing from bus i.
$\bar{S}_{li}$	Complex power of the load at bus i.
$\bar{S}_i$	Net complex power at bus i.
s_i	Apparent power capability of the inverter at bus i.
$\bar{V}_0$	Reference voltage (1 pu, zero angle) at bus 0.
$\boldsymbol{V_0}$	Vector containing $\|\bar{V}_0\|$ as elements of size $(n \times 1)$.

$\boldsymbol{V}$	Vector containing bus voltages of size ($n \times 1$).

DEDICATION

Dedicated to my affectionate mother, Siham Mustafa; my brothers, Nabil and Mohammad; my sisters, Ghada and Amaal, my roommate Eng. Hussam Al Shami and my best friends for their care and support.

Dedicated to the memory of my father, Nayef Mousa, who was deceased on November 18, 2016. It was the worst news I have ever heard, but you taught me to be strong and fight in life.

I hope you are still alive and share with me this achievement; I always remember your dream for me to be a Ph.D. holder; this is the second step, and I promise that I will aggressively seek to accomplish it whenever the chance arises. Thank you for being my father, my teacher in class, my friend, and my mentor.

CHAPTER I

INTRODUCTION

A. Problem Definition

The installed renewables worldwide, mainly solar and wind projects, are increasing at a rapid rate where it is estimated that a total capacity of 153 GW of renewable energy projects was installed in 2015 including about 500,000 photovoltaic panels and that saw renewables surpassing coal as the most significant source of power capacity. However, coal remains the largest supplier of the world's power with a share of 39% and renewables with 23% share [1]. Lebanon has followed the path of sustainable energy since the commitment launched by the Lebanese government to install and finance renewable energy projects in Copenhagen during the 2009 Conference of Parties meeting. The average production capacity in Lebanon in 2009 was 1500 MW with a total produced energy of 11522 GWh, while the average demand during the same year was 2400 MW of power and 15000 GWh of energy. This deficit has led the Government to take actions, and approving the Ministry of Energy and Water Policy Paper for the Electricity Sector in 2010 was a turning point which includes solutions at the generation, transmission and distribution levels [2], [3]. The plans have turned into actual projects with a total installed solar PV electricity of 9.45 MWp by 2015 and a total investment of $30.5 M [4]. According to the National Renewable

Energy Action Plan (NREAP) 2016-2020 [2], the set target is to reach by 2020 a production from renewable sources amounting to 12% of the projected total electricity and heating demand in Lebanon during that year, where solar photovoltaic distributed generation represents 4% of that 12% share. Integrating distributed photovoltaic generation with the distribution network may have adverse effects such as voltage flicker, introducing harmonics, altering short circuit levels and most importantly changing voltage levels and power flows [5], [6]. Voltage fluctuation beyond the acceptable levels can be caused by the varying generation levels from the PV generators. The rapidly varying irradiance levels impose a challenging problem on the distribution system because the currently installed regulation equipment like under load-tap changing transformers, step voltage regulators, and switched capacitors are slow; they cannot provide an adequate response to the fast varying generation levels. Initially, PV inverters were not allowed to regulate voltage levels [7], but according to a recent amendment to the IEEE 1547 interconnection standards [8], they are now required to absorb or supply reactive power to account for voltage sags and swells in the network, and that provides a new opportunity for optimizing the operation of distribution systems.

B. Literature Review

The problem of reactive power based voltage control can be classified into two main categories: centralized with the possibility of distributed computation, and decentralized (or local) [9]. The use of centralized control algorithms depends on the deployment of smart grid technologies which facilitate the fast exchange of voltage levels and power measurements, and thus allow the centralized optimization algorithms to dispatch the reactive power from PV inverters guaranteeing optimal solutions [10]. Reference [10] tackled the problem of integrating PV generation by proposing a centralized optimization algorithm with the objective of minimizing thermal losses while keeping voltage levels within constraints. The proposed algorithm is based on the Linearized Distribution Flow (LinDistFlow) equations that have been developed in [11]; results showed that it could achieve 20% reduction in losses. Reference [12] proposed an improved centralized control scheme by developing a convex relaxation of the Distribution Flow (DistFlow) equations in the formulation of the Volt/VAR control optimization problem, with the aim to minimize network losses and power consumption across the network. Another centralized optimal inverter dispatch has been proposed in [13] where the algorithm employs semidefinite relaxation techniques to determine the active and reactive power set points of critical PV inverters on the network. The work in [13] has also been developed into distributed optimal inverter dispatch (DOID) algorithms using the alternating direction method of multipliers, where the OID

problem is divided into sub-problems that can be solved locally to determine the inverters' set points. This approach has been improved by [14] that used a dual ε-subgradient method; results showed that the proposed controller could be employed in a distributed fashion where the optimal signals are updated at a faster rate than those introduced in [13], and speed of performance remains fast even when controlling a high number of PV systems.

On the other hand, the dependence on communication introduces a new vulnerability that may limit the applicability of centralized algorithms; thus decentralized control algorithms have been proposed which depend on local measurements of power and voltage levels. The local control scheme presented in [10] is based on reactive power consumption and achieved 80% of loss savings compared to the centralized control algorithm. Refs. [9], [15] have extended [10] by optimizing both the power losses and the voltage deviation; results showed that the optimal solution hinges on the appropriate choice of a weighting parameter that trades between the two objectives. Ref. [16] explained that the use of local voltage measurements is insufficient to maintain voltage within an acceptable range, and proposed two decentralized control algorithms that can achieve acceptable voltage levels for various operating conditions. Using also local measurements of active power production and voltage, [17] developed an active power dependent characteristic Q(P) curve that is in function of the produced PV active power levels; results showed that the proposed characteristic outperformed

the German Grid Code characteristics [17] in terms of reactive power consumption, power losses, and voltage regulation. The authors in [18] proposed a local controller to alleviate voltage rise using both reactive power compensation in addition to active power curtailment, where the use of the latter for up to 3% of the annual yield can increase the hosting capacity of the LV networks by about 50% [19].

Researchers have also studied the performance of coordinated control between PV inverters and other network components like capacitor banks, tap-changer transformers, and network configuration switches. Ref. [20] developed a dynamic control strategy for voltage regulation resulting in better performance compared to cosφ(P) and Q(V) control strategies, while [21] proposed a passive approach by regulating power factor and the transformer tap-changer settings to improve the system performance from transmission and distribution perspectives. Ref. [22] developed a mixed integer linear programming (MILP) tool to achieve minimum loss operation by coordinating the control of PV inverters, capacitor banks, and network configuration switches. The percentage of loss reduction obtained using the MILP tool surpassed those obtained using local control [10], which confirmed the effectiveness of coordinated control in power system optimization.

C. Thesis Contribution and Organization

This paper considers the local control of inverter reactive power via a Q(P) decision rule, in which the reactive power is a linear function of the real generated power along the lines of the solution suggested in [23]. The coefficients of the linear decision rule are computed using an affinely adjustable robust counterpart (AARC) approach [24]. Ref. [25] used the AARC approach for the optimal power flow under uncertain renewable energy resources. This optimization method can also be used here to account for uncertainty in the photovoltaic generation levels due to rapidly varying cloud transients; the result is an optimal local dispatch of reactive power from the PV inverters that leads to minimizing the maximum absolute voltage magnitude deviation from the nominal voltage level.

The rest of the thesis is organized as follows. Chapter II describes the mathematical modeling of the radial network used in this thesis, the governing power flow equations, in addition to the inverter capacity model. Chapter III introduces the robust optimization method and the application of the AARC approach in computing local decision rules that minimize the maximum absolute voltage magnitude deviation in distribution systems. Numerical results are presented in chapter IV, and the thesis is concluded in chapter V.

CHAPTER II

MATHEMATICAL MODELING

A. DistFlow Equations in a Radial Distribution System

To derive the governing power flow and voltage equations, consider the radial distribution system given in Fig. 1 with n nodes.

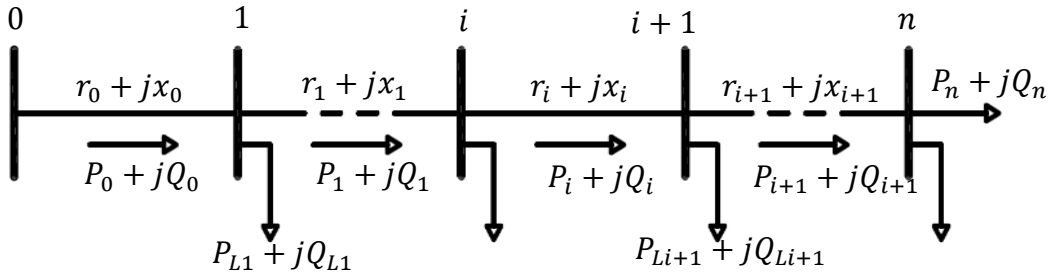

Fig.1. Radial distribution circuit diagram with notations of the power flow and complex impedance of lines.

The net complex power $P_{Li+1} + jQ_{Li+1}$ drawn at node $i + 1$ is composed of the local consumed power by the load minus the local produced PV power at that node (if any), i.e. $P_{Li+1} + jQ_{Li+1} = \left(p^c_{i+1} - p^g_{i+1}\right) + j\left(q^c_{i+1} - q^g_{i+1}\right)$.

From Fig. 1, the complex power $\bar{S}_1$ at node 1 can be expressed in terms of the complex substation power $\bar{S}_0$, the loss in the line between node 0 and node 1, and the net power drawn at node 1 as:

$$\bar{S}_1 = \bar{S}_0 - \bar{S}_{loss0} - \bar{S}_{L1} \tag{1}$$

The complex power loss can be expressed as:

$$\bar{S}_{loss0} = (r_0 + jx_0)\frac{|\bar{S}_0|^2}{|\bar{V}_0|^2} \quad (2)$$

Using (2), $\bar{S}_1$ can be written as:

$$\bar{S}_1 = \bar{S}_0 - (r_0 + jx_0)\frac{|\bar{S}_0|^2}{|\bar{V}_i|^2} - \bar{S}_{L1} \quad (3)$$

Equating the real and imaginary parts of (3) gives:

$$P_1 = P_0 - r_0\frac{({P_0}^2+{Q_0}^2)}{|\bar{V}_0|^2} - P_{L1} \quad (4)$$

$$Q_1 = Q_0 - x_0\frac{({P_0}^2+{Q_0}^2)}{|\bar{V}_0|^2} - Q_{L1} \quad (5)$$

Equations (4) and (5), which represent the real and imaginary power flow in the lines can be generalized to (6) and (7), which are known as the DistFlow power equations [9-11], [15]:

$$P_{i+1} = P_i - r_i\frac{({P_i}^2+{Q_i}^2)}{|\bar{V}_i|^2} - P_{Li+1} \quad (6)$$

$$Q_{i+1} = Q_i - x_i\frac{({P_i}^2+{Q_i}^2)}{|\bar{V}_i|^2} - Q_{Li+1} \quad (7)$$

The voltage at node 1 can be expressed in terms of the substation voltage $\bar{V}_0$ and the voltage drop in the line between node 0 and node 1 as:

$$\bar{V}_1 = \bar{V}_0 - (r_0 + jx_0)\frac{\bar{S}_0{}^*}{\bar{V}_0{}^*} \quad (8)$$

Using the complex numbers identities $|\bar{z}|^2 = z\bar{z}$ and $\overline{a+b} = \bar{a} + \bar{b}$, the voltage magnitude squared at node 1 can be written as:

$$|\bar{V}_1|^2 = \left[\bar{V}_0 - (r_0 + jx_0)\frac{\bar{S}_0{}^*}{\bar{V}_0{}^*}\right]\left[\bar{V}_0{}^* - (r_0 - jx_0)\frac{\bar{S}_0}{\bar{V}_0}\right] \quad (9)$$

By multiplying the terms on the right-hand side, (9) can be expressed as:

$$|\bar{V}_1|^2 = |\bar{V}_0|^2 - 2(r_0 P_0 + x_0 Q_0) + ({r_0}^2 + {x_0}^2)\frac{({P_0}^2 + {Q_0}^2)}{|\bar{V}_0|^2} \quad (10)$$

Equation (10) can be generalized to form the DistFlow voltage equation [9-11], [15]:

$$|\bar{V}_{i+1}|^2 = |\bar{V}_i|^2 - 2(r_i P_i + x_i Q_i) + ({r_i}^2 + {x_i}^2)\frac{({P_i}^2 + {Q_i}^2)}{|\bar{V}_i|^2} \quad (11)$$

B. Linearized DistFlow Equations

In practical networks, the complex power flow $\bar{S}_i = P_i + jQ_i$ in the lines is much greater than the losses, therefore a good approximation of the DistFlow equations is to drop the 2nd order quadratic terms corresponding to the losses [11], [15-16]. Following this assumption, the DistFlow equations can be linearized to form the LinDistFlow equations [11], [15-16] and expressed by:

$$P_{i+1} = P_i - P_{Li+1} \quad (12)$$

$$Q_{i+1} = Q_i - Q_{Li+1} \quad (13)$$

$$|\bar{V}_{i+1}|^2 = |\bar{V}_i|^2 - 2(r_i P_i + x_i Q_i) \quad (14)$$

The squared voltage in (14) is an independent variable. By approximating the voltage magnitude, $|\bar{V}_i|$ at any node i to 1pu [16], [26], the voltage equation (14) can be further reduced to:

$$|\bar{V}_{i+1}| = |\bar{V}_i| - (r_i P_i + x_i Q_i) \quad (15)$$

Based on (15), the difference in voltage magnitude between node 0 and node 2 can be found as follows:

$$|\bar{V}_0| - |\bar{V}_1| = r_0 P_0 + x_0 Q_0 \tag{16}$$

$$|\bar{V}_1| - |\bar{V}_2| = r_1 P_1 + x_1 Q_1 \tag{17}$$

$$|\bar{V}_0| - |\bar{V}_2| = r_0 P_0 + x_0 Q_0 + r_1 P_1 + x_1 Q_1 \tag{18}$$

Based on (12) and (13), the power flows P_i and Q_i in the lines can be expressed by:

$$P_i = \sum_{k \in d(i)} P_{Lk} = \sum_{k \in d(i)} (p_k^c - p_k^g) \tag{19}$$

$$Q_i = \sum_{k \in d(i)} Q_{Lk} = \sum_{k \in d(i)} (q_k^c - q_k^g) \tag{20}$$

Substituting (19) and (20) in (18) yields:

$$|\bar{V}_0| - |\bar{V}_2| = r_0\left[(p_1^c - p_1^g) + (p_2^c - p_2^g) + \cdots + (p_n^c - p_n^g)\right] + x_0\left[(q_1^c - q_1^g) + (q_2^c - q_2^g) + \cdots + (q_n^c - q_n^g)\right] + r_1\left[(p_2^c - p_2^g) + \cdots + (p_n^c - p_n^g)\right] + x_1[(q_2^c - q_2^g) + \cdots + (q_n^c - q_n^g)] \tag{21}$$

Rearranging (21) yields:

$$|\bar{V}_0| - |\bar{V}_2| = (p_1^c - p_1^g)(r_0) + (p_2^c - p_2^g)(r_0 + r_1) + \cdots + (p_n^c - p_n^g)(r_0 + r_1) + (q_1^c - q_1^g)(x_0) + (q_2^c - q_2^g)(x_0 + x_1) + \cdots + (q_n^c - q_n^g)(x_0 + x_1) \tag{22}$$

Equation (22) can be expressed by:

$$|\bar{V}_0| - |\bar{V}_2| = \sum_{j \in N} R_{2j}(p_j^c - p_j^g) + \sum_{j \in N} X_{2j}(q_j^c - q_j^g) \tag{23}$$

Therefore, the voltage at any node i can be expressed by (24) as [26]:

$$|\bar{V}_i| = |\bar{V}_0| + \sum_{j\in N} R_{ij}\left(p_j^g - p_j^c\right) + \sum_{j\in N} X_{ij}\left(q_j^g - q_j^c\right) \quad (24)$$

where R_{ij}, and X_{ij} can be found using (25) as illustrated in Fig. 2:

$$R_{ij} = \sum_{z\in L_i\cap L_j} r_z,\ X_{ij} = \sum_{z\in L_i\cap L_j} x_z \quad (25)$$

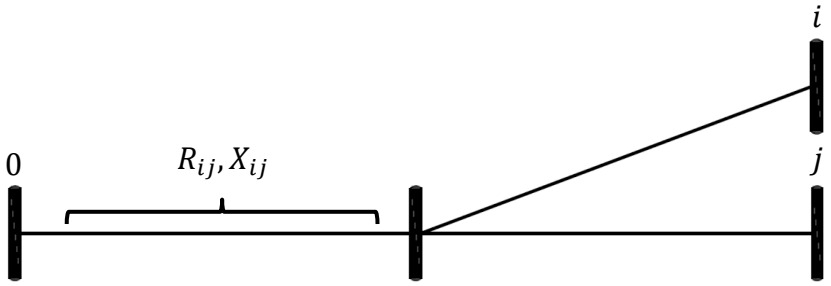

Fig. 2. Diagram demonstrating the definition of the R_{ij} and X_{ij} values.

Equation (24) can be written in matrix form as [26]:

$$\boldsymbol{V} = \boldsymbol{V_0} + \boldsymbol{R}(\boldsymbol{p^g} - \boldsymbol{p^c}) + \boldsymbol{X}(\boldsymbol{q^g} - \boldsymbol{q^c}) \quad (26)$$

where

$$\boldsymbol{R} = \left[R_{ij}\right]_{n\times n},\ \boldsymbol{X} = \left[X_{ij}\right]_{n\times n} \quad (27)$$

The $\boldsymbol{R}$, and $\boldsymbol{X}$ matrices could be alternatively computed starting from the $\boldsymbol{Y_{bus}}$ matrix as in (28); then $\boldsymbol{R} = re(\boldsymbol{inv}(\boldsymbol{Y_{bus}}))$, and $\boldsymbol{X} = imag(\boldsymbol{inv}(\boldsymbol{Y_{bus}}))$, where their 1st row and 1st column are set to zeros (here node 1 is considered as the substation bus conforming to the systems employed in numerical testing) as illustrated in (29) and (30):

$$\boldsymbol{Y_{bus}} = \begin{bmatrix} 1 & 0 & \dots & 0 \\ \bar{Y}_{21} & \bar{Y}_{22} & \dots & \bar{Y}_{2n} \\ \vdots & \vdots & \vdots & \vdots \\ \bar{Y}_{n1} & \bar{Y}_{n2} & \dots & \bar{Y}_{nn} \end{bmatrix} \tag{28}$$

$$\boldsymbol{R} = \begin{bmatrix} 0 & 0 & \dots & 0 \\ 0 & R_{22} & \dots & R_{2n} \\ \vdots & \vdots & \vdots & \vdots \\ 0 & R_{n2} & \dots & R_{nn} \end{bmatrix} \tag{29}$$

$$\boldsymbol{X} = \begin{bmatrix} 0 & 0 & \dots & 0 \\ 0 & X_{22} & \dots & X_{2n} \\ \vdots & \vdots & \vdots & \vdots \\ 0 & X_{n2} & \dots & X_{nn} \end{bmatrix} \tag{30}$$

C. Inverter Modeling

1. Inverter Capability Model

In this section, a simple inverter model previously used in [9-10], [15], and [23] is presented to determine the limitations for the inverter's reactive power contribution to the distribution system. According to a recent amendment to the IEEE 1547 interconnection standards [8], PV inverters are now required to contribute to voltage control by absorbing or supplying reactive power. The PV inverter's reactive power is limited by the capacity model shown in Fig. 3. From Fig. 3, the relation between the

inverter's apparent power capability s_i, real power generated p_i^g, and its reactive power q_i^g is expressed by:

$$\left|q_i^g\right| \leq \sqrt{{s_i}^2 - \left(p_i^g\right)^2} \tag{31}$$

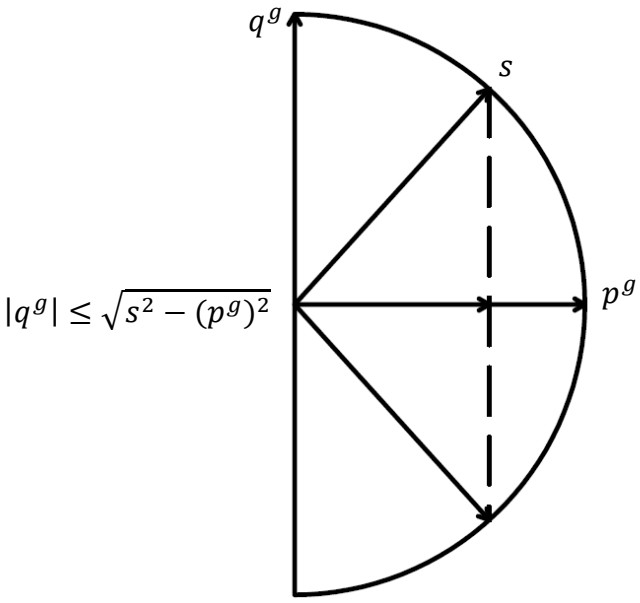

Fig. 3. Capability model of the inverter.

2. Linearized Inverter Capability Model

A good approximation of the capability model can be obtained by replacing it with the inscribed trapezoid having maximum area; thus the first step is to determine its coordinates on the capability model as shown in Fig. 4.

From Fig. 4, $b_1 = 2r$ and the area of the inscribed trapezoid is given by:

$$A = \frac{(b_1+b_2)h}{2} \tag{32}$$

Based on the drawn right triangles, r^2 is equal to:

$$r^2 = h^2 + (\frac{b_2}{2})^2 \tag{33}$$

Then, b_2 is equal to:

$$b_2 = 2\sqrt{r^2 - h^2} \tag{34}$$

Substituting b_1 and b_2 in (32) yields:

$$A = hr + h\sqrt{r^2 - h^2} \tag{35}$$

The maximum area of the inscribed trapezoid can be found by setting $\frac{dA}{dh} = 0$, thus:

$$r + \sqrt{r^2 - h^2} - \frac{h^2}{\sqrt{r^2-h^2}} = 0 \tag{36}$$

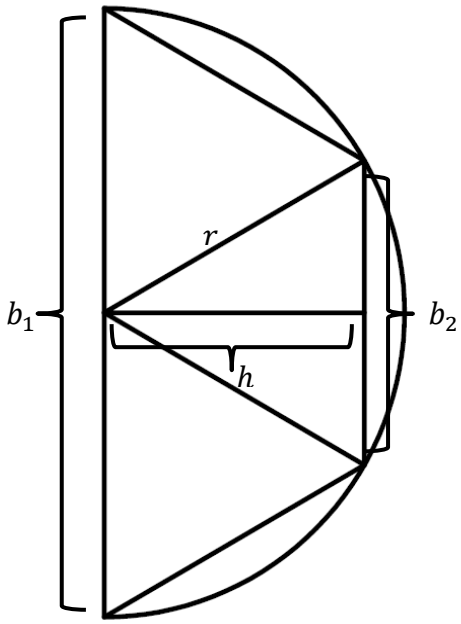

Fig. 4. Diagram demonstrating the inscribed trapezoid having maximum area.

Solving for h from (36) gives:

$$h = \frac{\sqrt{3}}{2} r \tag{37}$$

Substituting h in (34) results in

$$b_2 = \mathrm{r} \tag{38}$$

Expressing the derived coordinates in terms of inverter's parameters results in the linearized inverter capability model shown in Fig. 5. The equations of the sides of the trapezoid can be found as follows:

Equation of line a:-

$$p_i^g = 0 \tag{39}$$

Equation of line b:-

$$p_i^g = \frac{\sqrt{3}}{2} s_i \tag{40}$$

Equation of line c:-

$$q_i^g = -\frac{\sqrt{3}}{3} p_i^g + s_i \tag{41}$$

Equation of line d:-

$$q_i^g = \frac{\sqrt{3}}{3} p_i^g - s_i \tag{42}$$

Following this approximation, constraint (31) is replaced by (43)-(46):

$$p_i^g \geq 0 \tag{43}$$

$$p_i^g \leq \frac{\sqrt{3}}{2} s_i \tag{44}$$

$$q_i^g \leq -\frac{\sqrt{3}}{3} p_i^g + s_i \tag{45}$$

$$q_i^g \geq \frac{\sqrt{3}}{3} p_i^g - s_i \tag{46}$$

The choice of the inverter's apparent capability s_i was the subject of a recent study [10]; it was concluded that a value of s_i around 10% higher than the maximum real power $p_i^{g\,max}$ would allow for reactive power dispatching from the inverter without curtailing the real power that could be produced.

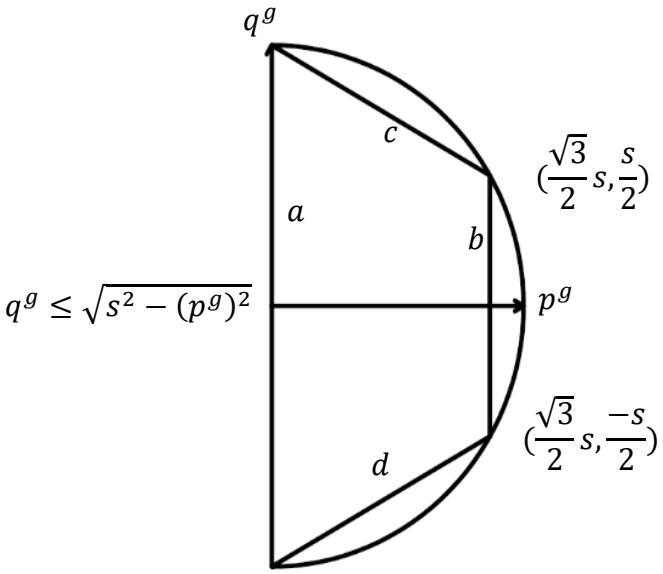

Fig. 5. Linearized inverter capability model.

CHAPTER III

METHODOLOGY

Robust Optimization (RO) is an optimization methodology that deals with uncertainty in the optimization parameters; it is appropriate when the uncertain parameters vary in a domain that is bounded and known, and when the constraints have to be satisfied for every value of the uncertain parameters in that domain. For instance, the uncertain parameters could be physical quantities such as temperature or pressure of approximate values obtained from a measuring device. A characteristic of RO is that it is a worst case oriented methodology. That is to say, if it is desired to get the optimal cost function that depends on a specific uncertain parameter, RO will give the supremum of the optimal cost of the instances. This, however, raises questions about the optimality of RO; it may give a cost which is far from optimal when the scenario is not the worst one. This has led to the development of adjustable robust counterpart (ARC) and affinely adjustable robust counterpart (AARC) approaches; they both give less conservative solutions than RO [24], as will be discussed in the next sections.

A. Robust Counterpart (RC)

Consider the following uncertain optimization problem:

$$\min_{\boldsymbol{x}}\{\boldsymbol{c^T x}: \boldsymbol{x} \in \boldsymbol{X}, f_i(\boldsymbol{x}, \xi_i) \geq 0\,, i = 1, \dots, m\}_{(\xi_1, \dots \xi_m) \in (\boldsymbol{Z_1} \times \dots \boldsymbol{Z_m})} \quad (47)$$

where $\boldsymbol{c} \in \boldsymbol{R^n}$ is a vector of constant coefficients, $\boldsymbol{X}$ is a convex and compact set, and the uncertain parameters are grouped in vector $\boldsymbol{\xi}$ whose elements belong to nonempty convex, compact and known uncertainty set $\boldsymbol{Z}$, i.e., $(\boldsymbol{\xi_1, \dots \xi_m}) \in (\boldsymbol{Z_1} \times \dots \times \boldsymbol{Z_m})$. The robust counterpart (RC) of problem (47) can be expressed as [27]:

$$\min_{\boldsymbol{x}}\left\{\boldsymbol{c^T x}: \boldsymbol{x} \in \boldsymbol{X}, \inf_{\xi_i \in Z_i} f_i(\boldsymbol{x}, \xi_i) \geq 0\,, i = 1, \dots, m\right\} \quad (48)$$

The best possible solution for every value of the uncertain parameter $\boldsymbol{\xi}$ can be found by solving the RC (48). According to the above formulation and before knowing the values of the uncertain parameters, all decision variables grouped in vector $\boldsymbol{x}$ have to be defined. However, in reality, part of the decision variables have to be defined before knowing the values of the uncertain parameters, and the others can adapt to the uncertain data. As a result, vector $\boldsymbol{x}$ is divided into non-adjustable variables $\boldsymbol{u}$ and adjustable variables $\boldsymbol{v}$. Thus, the RC can be expressed as (49) or equivalently as (50) [24]:

$$\min_{\boldsymbol{u},\boldsymbol{v}}\left\{\boldsymbol{c^T u}: (\boldsymbol{u}, \boldsymbol{v}) \in \boldsymbol{X}, \inf_{\xi_i \in Z_i} f_i(\boldsymbol{u}, \boldsymbol{v}, \xi_i) \geq 0\,, i = 1, \dots, m\right\} \quad (49)$$

$$\min_{\boldsymbol{u}}\{\boldsymbol{c^T u}: \exists \boldsymbol{v} \mid (\boldsymbol{u}, \boldsymbol{v}) \in \boldsymbol{X}, \forall i = 1, \dots, m, \forall\, (\xi_i \in Z_i),\ f_i(\boldsymbol{u}, \boldsymbol{v}, \xi_i) \geq 0\} \quad (50)$$

B. Adjustable Robust Counterpart (ARC)

A more flexible model than the RC is the adjustable robust counterpart (ARC); it has a larger feasibility set than the RC and thus allows achieving a better optimal value of the solution while satisfying the constraints for every value of the uncertain parameters. ARC is introduced in [28] as follows:

$$\min_{\boldsymbol{u}}\{\boldsymbol{c}^{\boldsymbol{T}}\boldsymbol{u}: \forall \boldsymbol{\xi} \in \boldsymbol{Z}, \exists \boldsymbol{v} \mid (\boldsymbol{u}, \boldsymbol{v}) \in \boldsymbol{X}, \forall i = 1, \dots, m, f_i(\boldsymbol{u}, \boldsymbol{v}, \xi_i) \geq 0\} \quad (51)$$

According to [28], the ARC of an uncertain linear optimization problem (52) can be expressed by (53):

$$\min_{\boldsymbol{u},\boldsymbol{v}}\{\boldsymbol{c}^{\boldsymbol{T}}\boldsymbol{u}: \boldsymbol{U}\boldsymbol{u} + \boldsymbol{V}\boldsymbol{v} \leq \boldsymbol{b}\}_{\boldsymbol{\xi} \equiv [\boldsymbol{U},\boldsymbol{V},\boldsymbol{b}] \in \boldsymbol{Z}} \quad (52)$$

$$\min_{\boldsymbol{u}}\{\boldsymbol{c}^{\boldsymbol{T}}\boldsymbol{u}: \forall (\boldsymbol{\xi} \equiv [\boldsymbol{U},\boldsymbol{V},\boldsymbol{b}] \in \boldsymbol{Z}), \exists \boldsymbol{v} \mid \boldsymbol{U}\boldsymbol{u} + \boldsymbol{V}\boldsymbol{v} \leq \boldsymbol{b}\} \quad (53)$$

where the data $\boldsymbol{\xi} \equiv [\boldsymbol{U},\boldsymbol{V},\boldsymbol{b}]$ varies in the uncertainty set $\boldsymbol{Z}$ and $\boldsymbol{V}$ is called the recourse matrix; the notation $\boldsymbol{\xi} \equiv [\boldsymbol{U},\boldsymbol{V},\boldsymbol{b}]$ implies that the elements in $[\boldsymbol{U},\boldsymbol{V},\boldsymbol{b}]$ are in general uncertain. Ref. [28] proved that ARC is a linear programming problem when the recourse matrix is fixed and set $\boldsymbol{Z}$ is a convex hull of scenarios; however, when $\boldsymbol{Z}$ is polytope defined by a list of linear inequalities, ARC can be NP hard.

C. Affinely Adjustable Robust Counterpart (AARC)

To look for more tractable approximations of the ARC, [28] introduced the concept of Affinely Adjustable Robust Counterparts (AARC) for a wider range of uncertainty sets. The AARC deals with linear problems, quadratic, and conic quadratic optimization problems [24]. Following [24], the AARC of the uncertain linear programming problem (52), is expressed as (54)-(55):

$$\min \boldsymbol{c^T u} \tag{54}$$

subject to

$$\boldsymbol{Uu + Vv \leq A\xi + b} \tag{55}$$

where $\boldsymbol{U}$, $\boldsymbol{V}$, $\boldsymbol{A}$, and $\boldsymbol{b}$ are fixed, and the adjustable variables $\boldsymbol{v}$ are considered affine (linear) dependent on the uncertain parameters $\boldsymbol{\xi}$ according to:

$$\boldsymbol{v = \alpha + \gamma\xi} \tag{56}$$

The dependency of the adjustable variables $\boldsymbol{v}$ as a function of the uncertain data is not definitely linear, however, in some cases, this dependency can be justified (see section 4.2 in [24] for the detailed discussion).

For a box constrained uncertainty set (57), (55) can be expressed for each row i by (58) as [24-25]:

$$\boldsymbol{\xi \in [\xi_{min}, \xi_{max}]} \tag{57}$$

$$\boldsymbol{U^i u + V^i \alpha - b^i + \max_{\xi \in [\xi^{min}, \xi^{max}]} [V^i \gamma - A^i]\, \xi \leq 0} \tag{58}$$

The maximization term in (58) is equivalent to:

$$\sum_{[\boldsymbol{V^i\gamma - A^i}]_j \geq 0} [\boldsymbol{V^i\gamma - A^i}]_j \xi_j^{max} + \sum_{[\boldsymbol{V^i\gamma - A^i}]_j < 0} [\boldsymbol{V^i\gamma - A^i}]_j \xi_j^{min} \tag{59}$$

$$= \sum_j \max([\boldsymbol{V^i\gamma - A^i}]_j, 0)\xi_j^{max} + \sum_j \min([\boldsymbol{V^i\gamma - A^i}]_j, 0)\xi_j^{min} \tag{60}$$

By making use of column vectors $\boldsymbol{\theta_i}$, $\boldsymbol{\varphi_i}$ of positive and negative slack variables respectively, the AARC can be finally written as the following LP:

$$\min_{\boldsymbol{u,\alpha,\gamma,\theta_i,\varphi_i}} \boldsymbol{c^T u} \tag{61}$$

subject to

$$\boldsymbol{U^i u + V^i w - b^i + \xi_{max}^T \theta_i + \xi_{min}^T \varphi_i} \leq 0 \tag{62}$$

$$\boldsymbol{\theta_i} \geq 0, \boldsymbol{\theta_i}^T \geq \boldsymbol{V^i\gamma - A^i} \tag{63}$$

$$\boldsymbol{\varphi_i} \leq 0, \boldsymbol{\varphi_i}^T \leq \boldsymbol{V^i\gamma - A^i} \tag{64}$$

The AARC seeks to find the optimal values of $\boldsymbol{\alpha}$ and $\boldsymbol{\gamma}$ corresponding to any value of $\boldsymbol{\xi}$, which is considered highly uncertain and varies according to the box constrained set defined by (57). The infinitely many constraints in (55) that corresponds to the infinite values of the uncertain parameter $\boldsymbol{\xi} \in [\boldsymbol{\xi_{min}}, \boldsymbol{\xi_{max}}]$ are reduced to linear inequalities by introducing slack column vector variables $\boldsymbol{\theta_i}$ and $\boldsymbol{\varphi_i}$. The detailed proof is presented in [24].

D. Affinely Adjustable Robust Counterpart Approach for Minimizing the Maximum Absolute Voltage Magnitude Deviation

The affinely adjustable robust counterpart (AARC) approach can be used here to account for uncertainty in the photovoltaic generation levels due to rapidly changing cloud transients; it computes the coefficients of the linear decision rule of the inverter reactive power, which is a linear function of the real generated power. The result is an optimal local dispatch of reactive power from the PV inverters that leads to minimizing the maximum absolute voltage magnitude deviation.

Minimizing the maximum absolute voltage magnitude deviation (65) that may occur at any node along the distribution system can be cast as a linear program (LP) with linear constraints (26) and (45)-(46):

$$\min \max \frac{1}{|\bar{V}_0|} \left| |\bar{V}_i| - |\bar{V}_0| \right| \tag{65}$$

By introducing a slack variable t with $\left||\bar{V}_i| - |\bar{V}_0|\right| \leq t$, (65) can be expressed as:

$$\min \frac{1}{|\bar{V}_0|} t \tag{66}$$

subject to

$$-t \leq |\bar{V}_0| - |\bar{V}_i| \tag{67}$$

$$-t \leq |\bar{V}_i| - |\bar{V}_0| \tag{68}$$

Equations (67)-(68) can be written in matrix form as:

$$-\boldsymbol{ones}(\boldsymbol{n}, \boldsymbol{1})t \leq \boldsymbol{V_0} - \boldsymbol{V} \tag{69}$$

$$-\boldsymbol{ones}(\boldsymbol{n}, \boldsymbol{1})t \leq \boldsymbol{V} - \boldsymbol{V_0} \tag{70}$$

Substituting (26) into (69)-(70) yields:

$$-\boldsymbol{ones}(\boldsymbol{n},\boldsymbol{1})t + \boldsymbol{Xq^g} \leq -\boldsymbol{Rp^g} + (\boldsymbol{Rp^c} + \boldsymbol{Xq^c}) \tag{71}$$

$$-\boldsymbol{ones}(\boldsymbol{n},\boldsymbol{1})t - \boldsymbol{Xq^g} \leq \boldsymbol{Rp^g} - (\boldsymbol{Rp^c} + \boldsymbol{Xq^c}) \tag{72}$$

The LP (65), (71)-(72) can be reformulated into the following standard form [24-25]:

$$\min \boldsymbol{c^T u} \tag{73}$$

subject to

$$\boldsymbol{Uu} + \boldsymbol{Vq^g} \leq \boldsymbol{Ap^g} + \boldsymbol{b} \tag{74}$$

where $\boldsymbol{c^T u}$ can be found by identification with (66) resulting in:

$$\boldsymbol{c^T} = \frac{1}{|\bar{V}_0|}, \boldsymbol{u} = t \tag{75}$$

Similarly, the matrices $\boldsymbol{U}$, $\boldsymbol{V}$, $\boldsymbol{A}$, and vector $\boldsymbol{b}$ can be found by identifying with constraints (45)-(46) and (71)-(72).

To simplify the expressions, define the following matrices:

$$\boldsymbol{N} = -\boldsymbol{ones}(\boldsymbol{n},\boldsymbol{1}), \boldsymbol{D} = -\frac{\sqrt{\boldsymbol{3}}}{\boldsymbol{3}}\boldsymbol{ones}(\boldsymbol{n},\boldsymbol{1}) \tag{76}$$

$$\boldsymbol{S_{n\times 1}} = [\boldsymbol{s_1} \ldots \boldsymbol{s_n}]^{\boldsymbol{T}}, \boldsymbol{I} = \boldsymbol{eye}(\boldsymbol{n}), \boldsymbol{Ze_{n\times 1}} = \boldsymbol{zeros}(\boldsymbol{n},\boldsymbol{1}) \tag{77}$$

where s_i in (77) is the inverter's apparent capability that is set equal to $1.1p_i^{gmax}$ as discussed in the linearized inverter capability model.

Using (76)-(77), the matrices $\boldsymbol{U}$, $\boldsymbol{V}$, $\boldsymbol{A}$, and vector $\boldsymbol{b}$ can be defined by:

$$\boldsymbol{U} = \begin{bmatrix} \boldsymbol{N} \\ \boldsymbol{N} \\ \boldsymbol{Ze} \\ \boldsymbol{Ze} \end{bmatrix}, \boldsymbol{V} = \begin{bmatrix} \boldsymbol{X} \\ -\boldsymbol{X} \\ \boldsymbol{I} \\ -\boldsymbol{I} \end{bmatrix}, \boldsymbol{A} = \begin{bmatrix} -\boldsymbol{R} \\ \boldsymbol{R} \\ \boldsymbol{diag}(\boldsymbol{D}) \\ \boldsymbol{diag}(\boldsymbol{D}) \end{bmatrix}, \boldsymbol{b} = \begin{bmatrix} (\boldsymbol{Rp^c} + \boldsymbol{Xq^c}) \\ -(\boldsymbol{Rp^c} + \boldsymbol{Xq^c}) \\ \boldsymbol{S} \\ \boldsymbol{S} \end{bmatrix} \tag{78}$$

The vector $\boldsymbol{p^g}$ represents the PV real power and $\boldsymbol{q^g}$ represents the reactive power generated from the PV inverters. The reactive power generated from the PV inverter is considered affine (linear) dependent on the PV real power according to the local control rule (79), which has been recently employed for mitigating the effect of solar power intermittency [23]:

$$q_i^g = \alpha_i + \gamma_i p_i^g \tag{79}$$

where α_i and γ_i are constants that are to be computed from solving the AARC (73)-(74). The AARC seeks to find the optimal values of α_i and γ_i corresponding to any value of p_i^g, which is considered highly uncertain and varies according to the box constrained set defined by (80):

$$p_i^g \in \left[0, p_i^{g^{max}}\right] \tag{80}$$

The lower and upper limits of (80) are calculated in accordance with (43)-(44). Given (80), (74) can be expressed for each row i as [24-25]:

$$\boldsymbol{U^i u} + \boldsymbol{V^i \alpha} - \boldsymbol{b^i} + \max_{\boldsymbol{p^g} \in [0, \boldsymbol{p^{gmax}}]} [\boldsymbol{V^i \gamma} - \boldsymbol{A^i}]\, \boldsymbol{p^g} \leq 0 \tag{81}$$

where $\boldsymbol{\alpha}$ is a column vector with values α_i and $\boldsymbol{\gamma}$ is a diagonal matrix with values γ_i on the diagonal.

The maximization term in (81) is equivalent to:

$$\sum_{[\boldsymbol{V^i \gamma} - \boldsymbol{A^i}]_j \geq 0} [\boldsymbol{V^i \gamma} - \boldsymbol{A^i}]_j p_j^{gmax}$$

$$= \textstyle\sum_j \max([\boldsymbol{V^i \gamma} - \boldsymbol{A^i}]_j, 0) p_j^{gmax} \tag{82}$$

By making use of column vectors $\boldsymbol{\theta_{i}}_{(n\times 1)}$ of positive slack, the AARC can be finally written as the following LP:

$$\min_{\boldsymbol{u},\boldsymbol{\alpha},\boldsymbol{\gamma},\boldsymbol{\theta}} \boldsymbol{c^{T}u} \tag{83}$$

subject to

$$\boldsymbol{U^{i}u} + \boldsymbol{V^{i}\alpha} - \boldsymbol{b^{i}} + \boldsymbol{p^{gmax^{T}}\theta_{i}} \leq 0 \tag{84}$$

$$\boldsymbol{\theta_{i}} \geq 0 \tag{85}$$

$$\boldsymbol{\theta_{i}}^{T} \geq \boldsymbol{V^{i}\gamma} - \boldsymbol{A^{i}} \tag{86}$$

CHAPTER IV

NUMERICAL RESULTS

The AARC formulation (83)-(86) was programmed in MATLAB, and CPLEX was used to solve the LP [29]. Tests were reported for two distribution networks; the 1st network shown in Fig. 6, is a lightly loaded 56-node distribution feeder modified from [30] with one large PV plant (5 MW) installed at node 45 away from the substation. The 2nd network shown in Fig. 7, is a 47-node distribution feeder modified from [12] with five PV plants of capacities (in MW): 1.5, 0.4, 1.5, 1, and 2 at nodes: 13, 17, 19, 23, 24. The networks data is available in the Appendix.

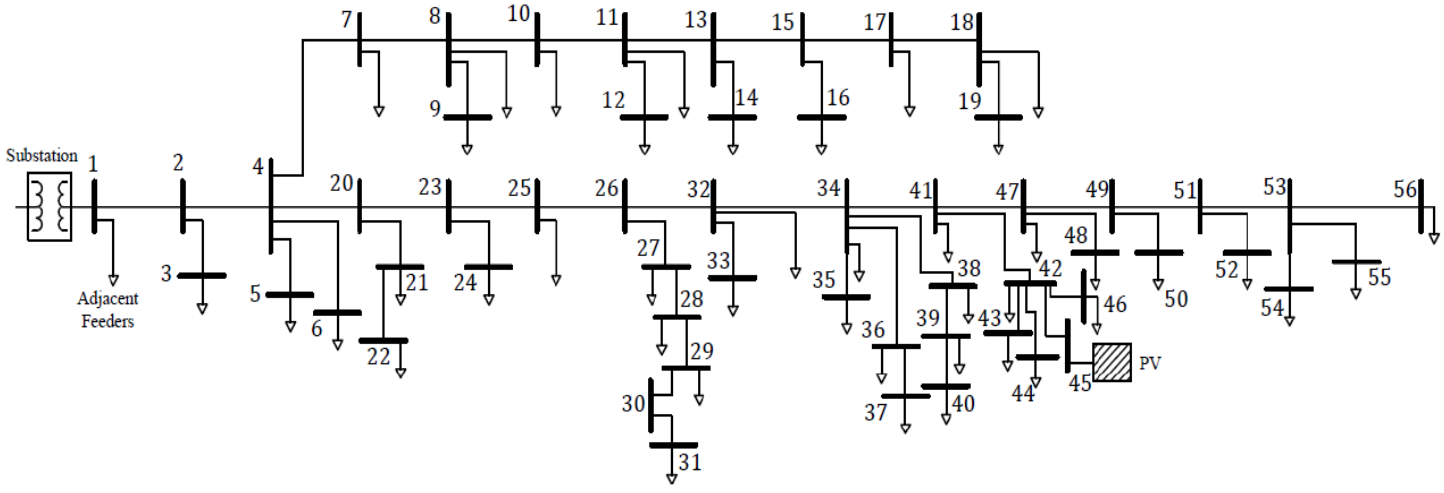

Fig. 6. Network diagram for Southern California Edison (SCE) distribution system.

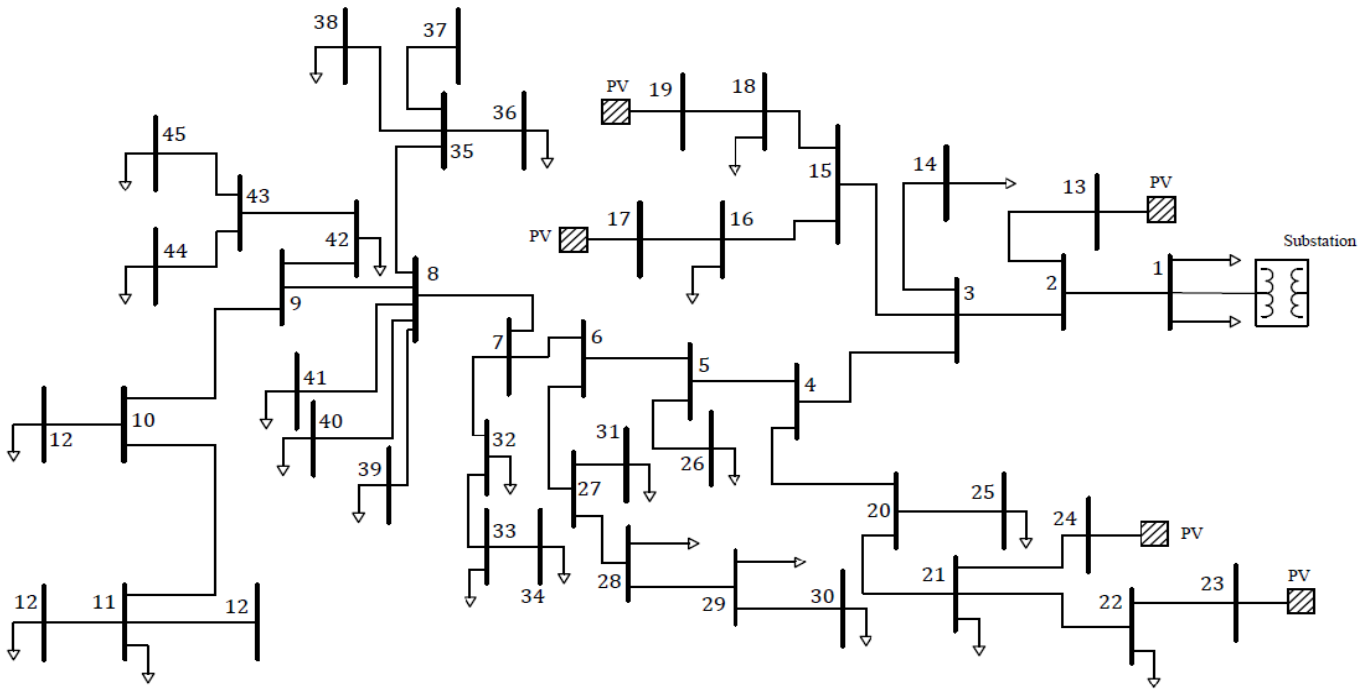

Fig. 7. Network diagram of the 47-node distribution feeder with high PV penetration.

The maximum absolute voltage magnitude deviation and power loss were calculated assuming that the reactive power generation from each PV inverter is given by the local control rule (79); the coefficients in (79) were obtained by solving the AARC (83)-(86). For 1st and 2nd networks, computing the decision rules via CPLEX [29] required 2.3 s and 1.3 s respectively, on a PC having 2.2 GHz Intel Core i7 processor with a memory of 8 GB. The computed coefficients of the linear decision rules are reported in TABLE I. These linear decision rules are used to determine the required reactive power from the PV inverters at the nodes having PV real power generation. Fig. 8 represents simulated PV real power generation for the 1st network and the corresponding inverter's reactive power. Similarly, for the 2nd network, the real and reactive power generation are represented in Figs. 9 and 10, respectively.

TABLE I. Coefficients of the Linear Decision Rules

Network #	**Inverter #**	α_i **(pu)**	γ_i
1	45	2.5708	-0.4170
2	13	1.65	-0.5774
	17	0.44	-0.5774
	19	1.65	-0.5774
	23	1.1	-0.5774
	24	2.2	-0.5774

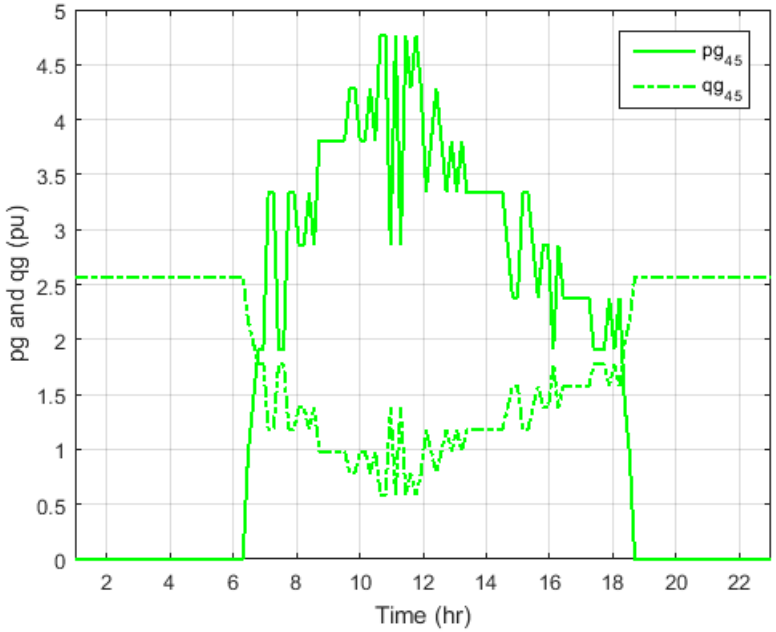

Fig. 8. Simulated PV real power generation for the 1st network and the corresponding inverter's reactive power.

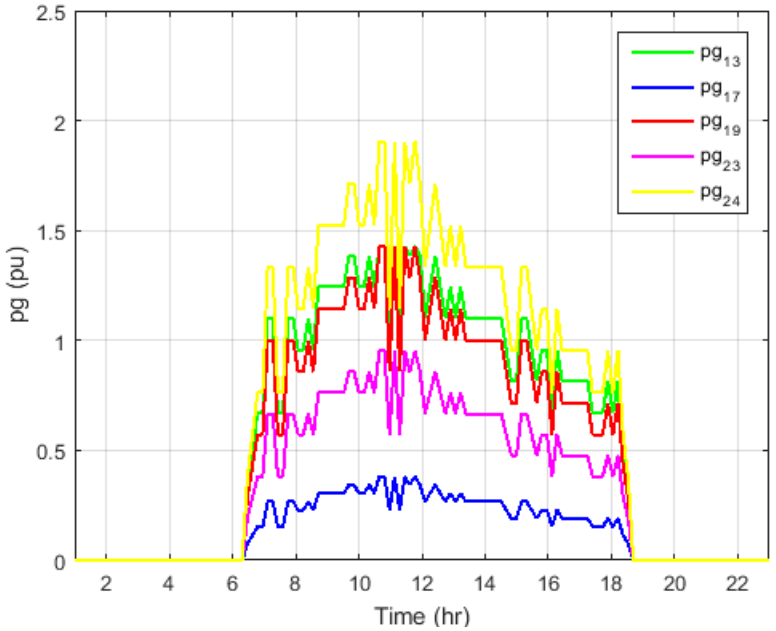

Fig. 9. Simulated PV real power generation for the 2nd network.

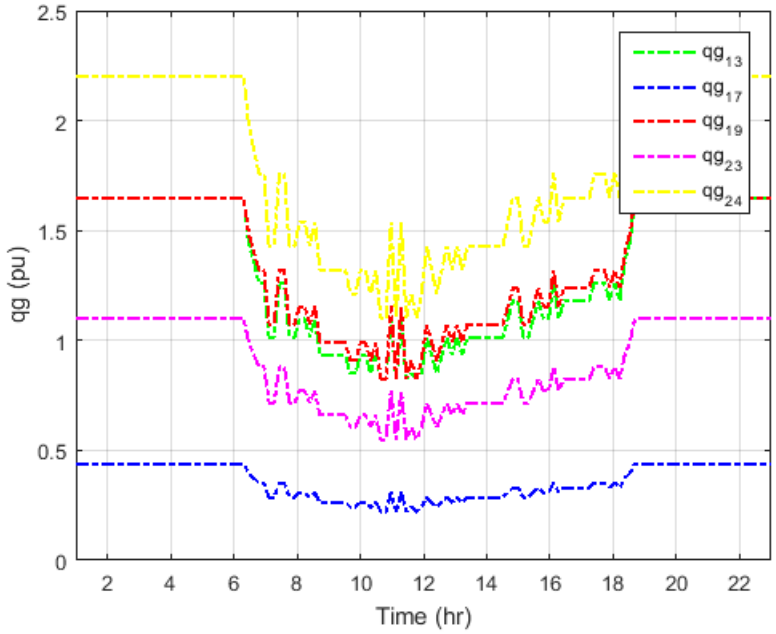

Fig. 10. Inverters' reactive power for the 2nd network.

A. Quantifying the Degree of Optimality of the Local Rules

To examine the optimality of the obtained results from the AARC formulation, a Monte-Carlo simulation with 10,000 trials was carried out; each trial corresponds to uniformly sampling values of PV real power from the box constrained set (80). The obtained values were used to calculate the maximum absolute voltage magnitude deviation using (26) and the power loss.

The power loss on each branch is equal to:

$$Power\ loss_{branch} = r_i|\bar{I}_i|^2 \tag{87}$$

where the magnitude of the current squared $|\bar{I}_i|^2$ can be found from:

$$|\bar{I}_i|^2 = \left|\left(\frac{\bar{S}_i}{\bar{V}_i}\right)^*\right|^2 = \frac{P_i^2+Q_i^2}{|\bar{V}_i|^2} \tag{88}$$

Following the LinDistFlow model discussed earlier, $|\bar{V}_i|$=1 pu is used as a first estimate; thus the real power loss per branch can be approximated by:

$$Power\ loss_{branch} = r_i(P_i^2 + Q_i^2)\ \text{pu} \tag{89}$$

Therefore, the power loss across all branches can be approximately calculated using [11]:

$$Power\ loss = \sum_{i=0}^{n_b} r_i(P_i^2 + Q_i^2)\ \text{pu} \tag{90}$$

The following 3 cases were considered:

1) ***Base Case (BC)***: the maximum absolute voltage magnitude deviation and power loss for each trial were calculated assuming no reactive power generation from the PV

inverters, i.e., the vector $\boldsymbol{q^g}$ is set to zero and the maximum absolute voltage magnitude deviation and power loss are calculated accordingly.

2) ***AARC*:** the maximum absolute voltage magnitude deviation and power loss for each trial were computed assuming that the reactive power is dispatched based on the linear decision rules whose coefficients are computed in TABLE I.

3) ***Centralized Control (CC)***: Assuming that the PV real power is measured at the PV generation nodes and sent to a centralized computer, the centralized computer solves the LP (91)-(92) in each Monte-Carlo Simulation ($\boldsymbol{p^g_{test}}$ is a column vector that represents the simulated PV generation values in each trial) for the optimal values of reactive power generation, and sends them back to the PV generation nodes for implementation. These calculated reactive generation values were used to obtain the maximum absolute voltage magnitude deviation and power loss.

$$\min \boldsymbol{f^T x} \tag{91}$$

subject to

$$\boldsymbol{Ax \leq b} \tag{92}$$

where

$$\boldsymbol{f^T} = \left[\frac{1}{|\bar{V}_0|},\ \boldsymbol{zeros(n,1)^T}\right],\ \boldsymbol{x} = \begin{bmatrix}\frac{1}{|\bar{V}_0|}\\ \boldsymbol{q^g}\end{bmatrix} \tag{93}$$

$$\boldsymbol{A} = \begin{bmatrix}\boldsymbol{N} & \boldsymbol{X}\\ \boldsymbol{N} & \boldsymbol{-X}\\ \boldsymbol{Ze} & \boldsymbol{I}\\ \boldsymbol{Ze} & \boldsymbol{-I}\end{bmatrix},\ \boldsymbol{b} = \begin{bmatrix}\boldsymbol{-R}\\ \boldsymbol{R}\\ \boldsymbol{diag(D)}\\ \boldsymbol{diag(D)}\end{bmatrix}\boldsymbol{p^g_{test}} + \begin{bmatrix}\boldsymbol{(Rp^c + Xq^c)}\\ \boldsymbol{-(Rp^c + Xq^c)}\\ \boldsymbol{S}\\ \boldsymbol{S}\end{bmatrix} \tag{94}$$

The comparison between the above 3 cases is reported in TABLE II. The comparison between the AARC solution and the centralized control was extended by calculating the percentage of improvement in the maximum absolute voltage magnitude deviation and power loss; the percentage improvement represents the percentage reduction of these values relative to the base case calculated as follows:

$$\%\ improvement\ in\ y = \frac{y_{BC} - y_{AARC\ or\ CC}}{y_{BC}} \times 100 \tag{95}$$

TABLE II. Maximum Absolute Voltage Magnitude Deviation and Power Loss from the Base Case, the AARC, and the Centralized Control

Network #	**Max $\|\Delta V\|_\infty$(pu)**			**Max Power Loss (kW)**			**Avg. Power Loss (kW)**		
	BC	***AARC***	***CC***	***BC***	***AARC***	***CC***	***BC***	***AARC***	***CC***
1	0.0613	0.0186	0.0186	123.74	113.05	113.05	62.94	57.24	57.21
2	0.0767	0.0436	0.0436	341.91	244.40	244.40	252.58	155.99	155.99

TABLE III. Percentage Improvement of the AARC and the Centralized Control Relative to the Base Case

Network #	**Max $\|\Delta V\|_\infty$**		**Max Power Loss**		**Avg. Power Loss**	
	AARC	***CC***	***AARC***	***CC***	***AARC***	***CC***
1	69.7	69.7	8.6	8.6	9.1	9.1
2	43.2	43.2	28.5	28.5	38.2	38.2

TABLE II shows that in the 1st network, the integration of the 5 MW plant led to a maximum absolute voltage magnitude deviation of 0.0613 pu, a maximum power loss of 123.74 kW, and an average power loss of 62.94 kW over 10,000 trials. The implementation of the AARC linear decision rules decreased the deviation to 0.0186 pu,

the maximum power loss to 113.05 kW, and the average power loss to 57.24 kW; this represents a reduction of 69.7%, 8.6%, and 9.1% from the base case respectively, as displayed in TABLE III. Similar and very close results were obtained when applying the centralized control which serves as an upper bound on the expected improvement from the AARC.

Similarly, for the 2nd network, TABLE II shows that the integration of the five PV plants gave a maximum absolute voltage magnitude deviation of 0.0767 pu, a maximum power loss of 341.91 kW, and an average power loss of 252.58 kW over 10,000 trials. The implementation of the AARC linear decision rules decreased the deviation to 0.0436 pu, the maximum power loss to 244.40 kW, and the average power loss to 155.99 kW; the corresponding percentages of improvement relative to the base case are given in TABLE III. The same results were obtained when applying the centralized control.

The above-reported results verify the degree of optimality associated with the AARC local control rules, and corroborate their effectiveness in reducing the maximum absolute voltage magnitude deviation in the system. It is worth mentioning that although the reduction of power loss is not in the objective function of the AARC, the power loss has been improved in both systems due to the reactive power support from the PV inverters.

B. Quantifying the Accuracy of the LinDistFlow Model

To examine the accuracy of the LinDistFlow model, the maximum absolute voltage magnitude deviation, the maximum power loss, and the average power loss (over 10,000 trials) were computed using (i) the LinDistFlow model and (ii) the MATPOWER AC power flow [31]. Also, a modeling error was computed as follows:

$$Modeling\ error = \frac{x_{MATPOWER} - x_{LinDistFlow}}{x_{LinDistFlow}} \times 100 \quad (96)$$

where x can represent the maximum absolute voltage magnitude deviation, the maximum power loss, or the average power loss; the results are reported in TABLES IV and V for all cases (base case, AARC, and the centralized control).

TABLE IV shows that in the 1st network, the AC power flow in the base case resulted in a maximum absolute voltage magnitude deviation of 0.0663 pu as compared to 0.0613 pu from LinDistFlow; for AARC and centralized control the deviation was 0.0203 pu from MATPOWER and 0.0186 pu from the LinDistFlow; this represents a modeling error of 8.2% for the base case and 9.1% for AARC/centralized control as displayed in TABLE V. The AC power flow resulted in a maximum power loss of 128.12 kW for the base case and 111.95 kW for AARC/centralized control, as compared to 123.74 kW and 113.05 kW from LinDistFlow; this represents a modeling error of 3.5% for the base case and -1% for AARC/centralized control (the negative percentage implies the value obtained from LinDistFlow is higher than the one obtained from MATPOWER) as shown in TABLE V. The average power loss (over 10,000

trials) was also employed to compute the corresponding modeling error as shown in TABLES IV and V. Similar results for the 2nd network are also reported in TABLES IV and V. These differences between the AC power flow and LinDistFlow are expected due to the approximations going into the LinDistFlow model.

According to the modeling error values shown in TABLE V, the LinDistFlow slightly underestimates the maximum absolute voltage magnitude deviation, and the linear decision rules when employed in the AC power flow simulation yield acceptable results.

TABLE IV. Maximum Absolute Voltage Magnitude Deviation and Power Loss from the Base Case, the AARC, and the Centralized Control using the LinDistFlow Model and MATPOWER

Network #	**LinDistFlow Model**			**MATPOWER**		
	Max $\|\Delta V\|_\infty$ (pu) **Max Power Loss (kW)** **Avg. Power Loss (kW)**			**Max $\|\Delta V\|_\infty$ (pu)** **Max Power Loss (kW)** **Avg. Power Loss (kW)**		
	BC	***AARC***	***CC***	***BC***	***AARC***	***CC***
1	0.0613 123.74 62.94	0.0186 113.05 57.24	0.0186 113.05 57.21	0.0663 128.12 67.78	0.0203 111.95 56.76	0.0203 111.95 56.73
2	0.0767 341.91 252.58	0.0436 244.40 155.99	0.0436 244.40 155.99	0.0844 404.51 295.18	0.0461 261.61 169.12	0.0461 261.61 169.12

TABLE V. Percentage Modeling Error from the LinDistFlow Model

Network #	**Max $\|\Delta V\|_\infty$**			**Max Power Loss**			**Avg. Power Loss**		
	BC	***AARC***	***CC***	***BC***	***AARC***	***CC***	***BC***	***AARC***	***CC***
1	8.2	9.1	9.1	3.5	-1.0	-1.0	7.7	-0.8	-0.8
2	10.0	5.7	5.7	18.3	7.0	7.0	16.9	8.4	8.4

CHAPTER V

CONCLUSION

The introduction of high penetration levels of PV generation into the distribution system necessitates the use of fast-reacting PV inverters for reactive power dispatching. This thesis presents an affinely adjustable robust counterpart approach for computing linear decision rules; these rules are then used locally to calculate the required reactive power support from the PV inverters for any value of generated real power. The methodology employs the LinDistFlow approximation of radial networks, and builds on recent advances in robust optimization theory. The results showed that the proposed control could significantly reduce the maximum absolute voltage magnitude deviation and at the same time reduce the power loss; in addition, comparison with centralized control on the available test instances suggest that the AARC decision rules are likely to give a maximum absolute voltage magnitude deviation that is very close to optimal. Validation was carried out with the AC power flow, and it showed that the AARC formulation that is based on the LinDistFlow model gives AC voltage levels that are within acceptable limits; in addition the power loss reduction as predicted by LinDistFlow holds to a good extent in the AC model. Future research directions include extending the approach to model meshed distribution networks, and coordinating the

decision rules for PV reactive power control with classical Volt-VAR optimization of switched capacitors and transformer taps.

APPENDIX

Modified Networks data of the systems presented in [30] and [12] respectively:

TABLE VI. Modified network data for Southern California Edison (SCE) distribution system

Network Data																	
Line Data				Line Data				Line Data				Load Data		Load Data		Load Data	
From Bus	To Bus	R (Ω)	X (Ω)	From Bus	To Bus	R (Ω)	X (Ω)	From Bus	To Bus	R (Ω)	X (Ω)	Bus #	Peak MVA	Bus #	Peak MVA	Bus #	Peak MVA
1	2	0.160	0.388	20	21	0.251	0.096	39	40	2.349	0.964	3	0.057	29	0.044	52	0.315
2	3	0.824	0.315	21	22	1.818	0.695	34	41	0.115	0.278	5	0.121	31	0.053	54	0.061
2	4	0.144	0.349	20	23	0.225	0.542	41	42	0.159	0.384	6	0.049	32	0.223	55	0.055
4	5	1.026	0.421	23	24	0.127	0.028	42	43	0.934	0.383	7	0.053	33	0.123	56	0.130
4	6	0.741	0.466	23	25	0.284	0.687	42	44	0.506	0.163	8	0.047	34	0.067	**Photovoltaic**	
4	7	0.528	0.468	25	26	0.171	0.414	42	45	0.095	0.195	9	0.068	35	0.094	**Bus #**	**Capacity (MW)**
7	8	0.358	0.314	26	27	0.414	0.386	42	46	1.915	0.769	10	0.048	36	0.097		
8	9	2.032	0.798	27	28	0.210	0.196	41	47	0.157	0.379	11	0.067	37	0.281	45	5
8	10	0.502	0.441	28	29	0.395	0.369	47	48	1.641	0.670	12	0.094	38	0.117	**Base Values and pf**	
10	11	0.372	0.327	29	30	0.248	0.232	47	49	0.081	0.196	14	0.057	39	0.131		
11	12	1.431	0.999	30	31	0.279	0.260	49	50	1.727	0.709	16	0.053	40	0.030		
11	13	0.429	0.377	26	32	0.205	0.495	49	51	0.112	0.270	17	0.057	41	0.046		
13	14	0.671	0.257	32	33	0.263	0.073	51	52	0.674	0.275	18	0.112	42	0.054		
13	15	0.457	0.401	32	34	0.071	0.171	51	53	0.070	0.170	19	0.087	43	0.083	V_{base} = 12 kV S_{base} = 1 MVA Z_{base} = 144 Ω pf = 0.9	
15	16	1.008	0.385	34	35	0.625	0.273	53	54	2.041	0.780	22	0.063	44	0.057		
15	17	0.153	0.134	34	36	0.510	0.209	53	55	0.813	0.334	24	0.135	46	0.134		
17	18	0.971	0.722	36	37	2.018	0.829	53	56	0.141	0.340	25	0.100	47	0.045		
18	19	1.885	0.721	34	38	1.602	0.406					27	0.048	48	0.196		
4	20	0.138	0.334	38	39	0.610	0.238					28	0.038	50	0.045		

TABLE VII. Modified network data of the 47-node distribution feeder with high PV penetration

Network Data																	
Line Data				Line Data				Line Data				Load Data		Load Data		Photovoltaic	
From Bus	To Bus	R (Ω)	X (Ω)	From Bus	To Bus	R (Ω)	X (Ω)	From Bus	To Bus	R (Ω)	X (Ω)	Bus #	Peak MVA	Bus #	Peak MVA	Bus #	Capacity (MW)
1	2	0.259	0.808	8	41	0.107	0.031	21	22	0.198	0.046	1	30	34	0.2	13	1.5
2	13	**	**	8	35	0.076	0.015	22	23	**	**	11	0.67	36	0.27	17	0.4
2	3	0.031	0.092	8	9	0.031	0.031	27	31	0.046	0.015	12	0.45	38	0.45	19	1.5
3	4	0.046	0.092	9	10	0.015	0.015	27	28	0.107	0.031	14	0.89	39	1.34	23	1
3	14	0.092	0.031	9	42	0.153	0.046	28	29	0.107	0.031	16	0.07	40	0.13	24	2
3	15	0.214	0.046	10	11	0.107	0.076	29	30	0.061	0.015	18	0.67	41	0.67		
4	20	0.336	0.061	10	46	0.229	0.122	32	33	0.046	0.015	21	0.45	42	0.13	**Base Values and pf**	
4	5	0.107	0.183	11	47	0.031	0.015	33	34	0.031	**	22	2.23	44	0.45		
5	26	0.061	0.015	11	12	0.076	0.046	35	36	0.076	0.015	25	0.45	45	0.2		
5	6	0.015	0.031	15	18	0.046	0.015	35	37	0.076	0.046	26	0.2	46	0.45		
6	27	0.168	0.061	15	16	0.107	0.015	35	38	0.107	0.015	28	0.13				
6	7	0.031	0.046	16	17	**	**	42	43	0.061	0.015	29	0.13			V_{base} = 12.35 kV S_{base} = 1 MVA Z_{base} = 152.52 Ω pf = 0.8 ** = 0.00001	
7	32	0.076	0.015	18	19	**	**	43	44	0.061	0.015	30	0.2				
7	8	0.015	0.015	20	21	0.122	0.092	43	45	0.061	0.015	31	0.07				
8	40	0.046	0.015	20	25	0.214	0.046					32	0.13				
8	39	0.244	0.046	21	24	**	**					33	0.27				

REFERENCES

[1] P. Clark, “Renewables overtake coal as world’s largest source of power capacity,” Financial Times, 2016, Available: https://www.ft.com/content/09a1f984-9a1d-11e6-8f9b-70e3cabccfae.

[2] Lebanese Center for Energy Conservation (LCEC), “The national renewable energy action plan for the republic of Lebanon 2016-2020,” Ministry of Energy and Water/ Lebanese Center for Energy Conservation (LCEC), 2016.

[3] Lebanese Center for Energy Conservation (LCEC), “The second national energy efficiency action plan for the republic of Lebanon: NEAP 2016-2020,” Ministry of Energy and Water/ Lebanese Center for Energy Conservation (LCEC), 2016.

[4] J. Amine and S. Rizk, “2015 solar PV status report for Lebanon,” UNDP/DREG - 2016.

[5] P. Barker and R. D. Mello, “Determining the impact of distributed generation on power systems part 1-radial distribution systems,” in IEEE Power Energy Soc. (PES) Sum. Meeting, vol. 3. Seattle, WA, USA, 2000, pp. 1645-1656.

[6] C. L. Masters, “Voltage rise: the issue when connecting embedded generation to long 11kV overhead lines,” Power Eng. J., vol. 16, no. 1, pp. 5-12, 2002.

[7] “IEEE standard for interconnecting distributed resources with electric power systems,” IEEE Std 1547-2003, pp. 1–28, July 2003.

[8] “IEEE standard for interconnecting distributed resources with electric power systems - amendment 1,” IEEE Std 1547a-2014 (Amendment to IEEE Std 1547-2003), pp. 1–16, May 2014.

[9] K. Turitsyn, P. Sulc, S. Backhaus, and M. Chertkov, “Options for control of reactive power by distributed photovoltaic generators,” Proc. of the IEEE, vol. 99, no. 6, pp. 1063–1073, Jun. 2011.

[10] K. Turitsyn, P. Sulc, S. Backhaus, and M. Chertkov, “Distributed control of reactive power flow in a radial distribution circuit with high photovoltaic penetration,” in IEEE PES General Meeting, Jul. 2010, pp. 1–6.

[11] M. Baran and F. Wu, “Network reconfiguration in distribution systems for loss reduction and load balancing,” IEEE Trans. Power Deliv., vol. 4, no. 2, pp. 1401-1407, Apr. 1989.

[12] M. Farivar, C. R. Clarke, S. H. Low, and K. M. Chandy, “Inverter VAR control for distribution systems with renewables,” in IEEE International Conference on Smart Grid Communications, Oct. 2011, pp. 457–462.

[13] E. Dall'Anese, S. V. Dhople, B. B. Johnson, and G. B. Giannakis, “Decentralized optimal dispatch of photovoltaic inverters in residential distribution systems,” IEEE Trans. Energy Conv., vol. 29, no. 4, pp.957–967, Dec. 2014.

[14] E. Dall'Anese, S. V. Dhople, and G. B. Giannakis, “Photovoltaic inverter controllers seeking AC optimal power flow solutions,” IEEE Trans. Power Syst., vol. 31, no. 4, pp. 2809–2823, Jul. 2016.

[15] K. Turitsyn, P. Sulc, S. Backhaus, and M. Chertkov, “Local control of reactive power by distributed photovoltaic generators,” in First IEEE International Conference on Smart Grid Communications, Oct. 2010, pp. 79–84.

[16] N. Li, G. Qu, and M. Dahleh, “Real-time decentralized voltage control in distribution networks,” in 52nd Annual Allerton Conference on Communication, Control, and Computing, Sep. 2014, pp. 582–588.

[17] A. Samadi, R. Eriksson, L. Soder, B. G. Rawn, J. C. Boemer, “Coordinated active power-dependent voltage regulation in distribution grids with PV systems,” IEEE Trans. Power Deliv., vol. 29, no. 3, pp. 1454–1464, Jun. 2014.

[18] F. Olivier, P. Aristidou, D. Ernst, T. Van Cutsem, “Active management of low-voltage networks for mitigating overvoltages due to photovoltaic units,” IEEE Trans. Smart Grid, vol. 7, no. 2, pp. 926–936, Mar. 2016.

[19] B. Bletterie, S. Kadam, R. Bulgarian, and A. Zegers, “Voltage control with PV inverters in low voltage networks-in depth analysis of different concepts and parameterization criteria,” IEEE Trans. Power Syst., vol. 32, no. 1, pp. 177–185, Jan. 2017.

[20] A. R. Malekpour and A. Pahwa, “A dynamic operational scheme for residential PV smart inverters,” IEEE Trans. Smart Grid, vol. PP, no. 99, pp. 1–10, 2016.

[21] A. Keane, L. F. Ochoa, E. Vittal, C. J. Dent, and G. P. Harrison, “Enhanced utilization of voltage control resources with distributed generation,” IEEE Trans. Power Syst., vol. 26, no. 1, pp. 252–260, Feb. 2011.

[22] R. A. Jabr, “Minimum loss operation of distribution networks with photovoltaic generation,” IET Renew. Power Gener, vol. 8, no. 1, pp. 33–44, Jan. 2014.

[23] W. Lin, R. J. Thomas, and E. Bitar, “Real-time regulation in distribution systems via decentralized PV inverter control,” in Proceedings of the 51st Hawaii International Conference on System Sciences, pp. 1–10, 2018.

[24] V. Guigues, “Robust production management,” Optimization and Engineering, vol. 10, no. 4, pp. 505–532, 2009.

[25] R. A. Jabr, “Adjustable robust OPF with renewable energy sources,” IEEE Trans. Power Syst., vol. 28, no. 4, pp. 4742–4751, Nov. 2013.

[26] M. Farivar, L. Chen, and S. Low, “Equilibrium and dynamics of local voltage control in distribution systems,” in 52nd IEEE Conference on Decision and Control, Florence, Italy, Dec. 2013, pp. 4329 – 4334.

[27] Ben-Tal A, Nemirovski A., “Robust convex optimization,” Math Oper. Res., vol. 23, no. 4, pp.769 –805, 1998.

[28] Ben-Tal A, Goryashko A., Guslitzer E., Nemirovski A., “Adjustable robust counterpart of uncertain linear programs,” Math Program 99, pp.351 –376, 2004.

[29] “IBM ILOG CPLEX. Ver. 12.7.1,” https://www.ibm.com/products/ilog-cplex-optimization-studio.

[30] M. Farivar, R. Neal, C. Clarke, and S. Low, “Optimal inverter VAR control in distribution systems with high PV penetration,” IEEE Power and Energy Society General Meeting, pp. 1–7, 2012.

[31] R. D. Zimmerman, C. E. Murillo-Sánchez, and R. J. Thomas, “MATPOWER: steady-state operations, planning and analysis tools for power systems research and education,” IEEE Trans. Power Syst. vol. 26, no. 1, pp. 12-19, Feb. 2011.